RADIANT HEAT EXCHANGE IN A SPACE ENVIRONMENT

Research and Development Contract No. 951661
California Institute of Technology
Jet Propulsion Laboratory
4800 Oak Grove Drive
Pasadena, California

University of Illinois Budget Code: 46-22-40-352

Scientific Technical Report No. 5

Period Covered: February 1, 1969, to July 31, 1969

Prepared by: R. G. Hering
A. F. Houchens
T. F. Smith
W. D. Fischer

Submitted by: R. G. Hering
Professor of Mechanical Engineering
266 Mechanical Engineering Building
University of Illinois at Urbana-Champaign
Urbana, Illinois 61801
Phone: Area Code 217, 333-0366

Date: July 31, 1969

TABLE OF CONTENTS

1. OBJECTIVES AND SCOPE

Studies are being conducted to develop analytical methods for predicting radiant heat transfer and temperature of engineering surfaces in a space environment. These studies include two major aspects. First, by thoroughly investigating the influence of directional and spectral property dependencies of engineering materials on radiant heat transfer and temperature by means of detailed analysis, the accuracy of present calculation methods may be assessed, new and improved methods developed, and the surface property data required to implement the new methods delineated. Second, since the results of analysis are only as valid as the surface property models employed, a facility is under development to measure bidirectional reflectance of surfaces with the aim of justifying and refining a bidirectional reflectance model for metallic engineering surfaces.

In Section 2 the progress made during a fifth six-month period of the contract is summarized and the current status of the research program reviewed. The anticipated progress for the next six-month period is discussed in Section 3.

2. CURRENT STATUS

The progress made and current status of the research program are reviewed under three major categories. Advances in the theoretical heat transfer effort are reported in Section 2.1. Section 2.2 is devoted to further analytical efforts to establish realistic radiation property models for engineering surfaces. Measurements of bi-directional reflectance in the plane of incidence for representative roughened metal samples are reported in Section 2.3.

2.1 RADIANT HEAT TRANSFER ANALYSIS

2.1.1 Radiant Heat Transfer for Non-gray, Non-diffuse Surfaces in a Space Environment

Calculations which account for real surface property effects on radiant heat transfer and equilibrium temperature for interacting surfaces in a space environment have been completed. The results are being compared to calculations employing simple surface property models for radiative transfer. The comparison is providing a means for assessing the extent to which present design techniques account for real surface effects and estimates of the magnitude of the error in heat flux and equilibrium temperature incurred by the use of simple property models. The real surface calculations also point out the level of radiation surface property detail required in radiant heat transfer calculations to assure acceptable design accuracy and delineate the surface property measurements necessary to implement improved thermal design methods.

Numerical results for radiant heat transfer in the absence of a solar flux and for equilibrium temperature of radiatively adiabatic surfaces in a solar field were only recently completed. Similar results have been obtained for simple surface property models and compromise models which attempt to retain the computational simplicity of simple models yet partially account for important real surface characteristics. All results are being studied for significant trends. The details of the calculations and the resulting conclusions will be the subject of a forthcoming report. Upon completion, this report will be submitted under separate cover.

2.1.2 Radiant Heat Transfer and Equilibrium Temperature of Surfaces with One-dimensional Roughness

Apparent thermal radiation properties for surfaces with one-dimensional V-groove roughness elements have been developed [1,2]*. These properties were derived employing concepts of geometrical optics and apply for optical roughness values in excess of unity. Analysis is under way to utilize the apparent properties to study the influence of directional emission and reflection on heat transfer and on equilibrium temperature of surfaces in a space environment. Studies are in various stages of completion for both isolated surfaces and systems of radiatively interacting surfaces. These studies complement those cited in Section 2.1.1 which employ a

*Numbers in brackets refer to entries in REFERENCES.

bidirectional reflectance model appropriate to surfaces with small optical roughness.

2.1.2.1 Isolated Surfaces

In an earlier report [2], preliminary results illustrating the influence of surface roughness on heat transfer and on the temperature acquired by an isolated radiatively adiabatic surface in a solar flux were presented. Two manuscripts have been prepared and submitted to technical journals. The first entitled SURFACE ROUGHNESS EFFECTS ON EQUILIBRIUM TEMPERATURE has been accepted for publication by Journal of Spacecraft and Rockets. Upon receipt, reprints of the published article will be submitted to JPL. The second manuscript entitled SURFACE ROUGHNESS EFFECTS ON RADIANT HEAT TRANSFER is under review.

2.1.2.2 Interacting Surfaces

Analysis and numerical results have been completed describing the influence of one-dimensional surface roughness on radiant heat transfer for interacting surfaces in the absence of external radiation fields. The system selected for study was identical equal-length adjoint plates of infinite width. Both surfaces have the same uniform temperature and surface properties were taken independent of temperature and wavelength. Preliminary heat flux results were reported earlier [3]. A manuscript has been prepared describing the details of the analysis, numerical results and conclusions.

The manuscript has been submitted to a technical journal for publication. Reprints of the article will be submitted to JPL upon receipt. A short summary of the important conclusions resulting from this study is provided in the next paragraph.

Surface roughness effects are for the most part unimportant for high emittance materials ($\varepsilon \geq 0.9$). The influence of surface roughness on radiant heat transfer steadily increases as material emittance values diminish. Surface roughness slope is more important than roughness element specularity in influencing radiant transfer for low emittance materials and can cause changes in local flux and total heat transfer rates as large as a factor of two. Of the simple diffuse and specular surface property models, rough surface local flux and total heat transfer is generally approximated most accurately by the diffuse emission-diffuse reflection model employing rough surface apparent emittance for hemispherical emittance. The error incurred in using this model to evaluate local flux for low to intermediate values of emittance, however, can be as large as 50 percent.

The analysis briefly described above has been extended to a second system of surfaces consisting of finite width parallel plates. This system may be varied between situations in which interreflections are negligible to those where radiant interaction is dominant. The analysis has also been extended to include not only the evaluation of local radiant flux, but net radiant exchange between the surfaces. The latter quantity is important in situations where the

net transfer of radiant energy from a source to a sink is of prime interest. A computer code has been written and verified. Numerical results are beginning to be realized, but are not yet sufficient in quantity to merit reporting.

Analysis has been completed extending that developed for the adjoint plate system to include solar flux and, hence, evaluation of surface roughness effects on equilibrium temperature of radiatively adiabatic surfaces. A code is under development to implement the acquisition of quantitative results.

2.1.3 Spectral Surface Property Effects on Radiant Transfer

An analysis has been completed which provides a mechanism for study of spectral surface property effects on radiant heat transfer between radiatively interacting surfaces. The system of surfaces initially chosen for study is the adjoint plate system in the absence of external thermal radiation fields. One of the purposes of this analysis is to provide information which can be utilized to delineate the relative importance of spectral and directional real surface property dependencies. Furthermore, additional information is required to ascertain the magnitude of the error incurred in gray and semigray methods of analysis. Initially, available spectral property measurements for selected materials will be employed in the calculations. Later the code capability is expected to be extended to include more general spectral property models. These models characterize the spectral dependence of classes of materials

in terms of a limited number of characteristic parameters. Results are not yet available.

2.2 RADIATION PROPERTY ANALYSIS

The study of the apparent radiation properties of surfaces with one-dimensional roughness elements in the shape of a V-groove was recently presented at the AIAA Fourth Thermophysics Conference at San Francisco, California. The paper is under review for publication in the conference proceedings. Reprints of the paper presented at the conference have been submitted to JPL and reprints of the published article will be sent upon receipt.

2.3 BIDIRECTIONAL REFLECTANCE MEASUREMENTS

In this section, plane of incidence BDR* measurements are presented for selected metal samples. Although the surface characteristics are not well-documented and the measurements are limited in quantity and scope, the measurements furnish information which is necessary to carry out the detailed study. First, techniques available to the investigators for surface preparation and specification were investigated. Second, signal levels of solid angle-slit width combinations for minimum detectable energy were determined. Third, techniques for efficient data acquisition and reduction were developed. Finally, the BDR measurements were compared with a BDR model

*Throughout Section 2.3, BDR is used as an abbreviation for bidirectional reflectance.

to develop techniques for such comparisons. In addition, the measurements helped define the capabilities and limitations of the reflectometer. The coordinate system to which all measurements are referred is shown in Fig. 1.

2.3.1 Test Samples

Test samples selected for study were six 6061-T6 aluminum alloy discs of 1/4-inch thickness and one-inch diameter. Samples were polished to a smooth finish and then finished to various degrees of roughness by utilizing standard polishing techniques with grits of different sizes. Sample designations and the grit sizes used in finishing of each sample are given in TABLE 1. The columns labeled σ and m are discussed later. Visual inspection reveals that sample roughness increases with increasing sample number designation. After roughening, each sample was cleaned and then coated with a vacuum deposited layer of pure aluminum to a thickness of approximately 1000 Å. This layer thickness retains the roughness of the aluminum alloy base metal while providing samples with the well-documented optical properties of pure aluminum. An attempt to obtain a quantitative measure of surface roughness by microinterferometer photographs met with only limited success. The photographs indicated only that samples designated 1 through 3 were nearly optically smooth while the other samples were too rough to obtain a meaningful roughness measurement by this technique. Other methods for determining surface roughness parameters were not available. Sample 1 was retained

as the smooth sample, and BDR measurements are reported only for samples 4, 5, and 6.

2.3.2 Measurements

2.3.2.1 Specular Reflectance

Monochromatic specular reflectance measurements relative to that of the smooth sample were acquired for wavelengths in the range 1-14 μm for an angle of incidence equal to 10°. The specular reflectance measurements for the samples designated 4, 5, and 6 are illustrated in Fig. 2b as a function of the wavelength of the incident energy. The solid and broken curves are discussed in Section 2.3.3. The ordinate represents the ratio of the reflectance of the roughened sample in the specular reflection direction, $\rho_s(\theta',\phi')$, to the corresponding value for the smooth sample, $\rho_o(\theta',\phi')$.

Certain characteristics of the measurements are apparent from this figure.

1. As wavelength increases, specular reflectance of the rough surface approaches that of the smooth surface. The implication is that with increasing wavelength, a rough surface reflects greater portions of the incident energy into the specular direction and, therefore, approaches a specular reflector. This behavior is more noticeable for the smoothest sample (4) than for the roughest sample (6).

2. At a fixed wavelength, the specular reflectance decreases with increasing rms surface roughness height. Two possible explanations can be given for this behavior. First, as roughness increases, the surface tends to scatter larger amounts of incident energy with a consequent reduction in specular reflectance. Second, multiple reflections within and between roughness asperities which decrease the magnitude

of reflected energy become more important as roughness height increases. A better understanding of this characteristic may be obtained by observing the variation of directional hemispherical reflectance with increasing roughness. If monochromatic directional hemispherical reflectance remains essentially invariant with increasing roughness, then the first explanation is appropriate. However, if it varies, both explanations could apply. Unfortunately, monochromatic directional hemispherical reflectance measurements of the samples were not available.

3. For wavelengths less than 4 μm, the specular reflectance for sample 6 is nearly independent of wavelength. A similar but not as noticeable trend is evident for sample 5 while this behavior is not apparent for sample 4.

The first two characteristics are similar to those predicted by BDR models based on physical optics. Thus, it appears that these models could be employed to correlate the reflectance measurements for wavelengths greater than 4 μm. The lack of a strong wavelength dependence of the specular reflectance measurements as illustrated by the last characteristic suggests that the reflectance measurements for wavelengths less than 2 μm should be correlated by models based on the concepts of geometrical optics. However, additional measurements are necessary to verify the third characteristic, particularly for wavelengths less than 2 μm. Trends similar to those observed have been reported in [4,5,6,7].

2.3.2.2 Bidirectional Reflectance

Plane of incidence BDR measurements were acquired for samples 4, 5, and 6 at an angle of incidence of 10° and wavelengths of 1.4, 2.4, 6.4, and 10.0 μm. Results are presented in Figs. 3,

4, and 5 for samples 4, 5, and 6, respectively. Results for sample 4 at 10.0 μm are not included since they were essentially identical to those shown in Fig. 3c for 6.4 μm. The solid and broken curves shown in these figures are discussed in Section 2.3.3. The ordinate $\overline{R}$ represents the ratio of the product of the BDR and the cosine of the angle of reflection to the corresponding product in the specular direction. Some trends are evident in these figures. First, all samples exhibit large reflectance values in a direction at or near that for specular reflection. Second, with increasing wavelength, each sample becomes increasingly specular. Third, for a fixed wavelength and increasing roughness, greater amounts of reflected energy are observed in directions other than the specular direction. Finally, the distributions for sample 5 at wavelengths of 1.4 μm and 2.4 μm are nearly identical. The first three trends are similar to those predicted by a physical optics BDR model while the fourth trend is similar to that predicted by a geometrical optics BDR model. No explanation is offered at this time for the data exceeding unity for sample 6 at a wavelength of 1.4 μm.

The BDR measurements shown in Figs. 3, 4, and 5 indicate that the samples are nearly specular reflectors, particularly for longer wavelengths. However, the difficulty in ascertaining if a surface is a specular reflector from these measurements can be illustrated by an example. Consider a surface with 10 percent of the reflected energy contained in the specular direction and the remaining 90 percent distributed diffusely over hemispherical space. The value of

$\overline{R}$ for directions other than near the specular direction is approximately 0.005 which if plotted to the scale shown in Fig. 3 would indicate that the surface is a specular reflector. Thus, normalizing the measurements with respect to that obtained in the specular direction gives only limited information concerning the spatial distribution of a large portion of the reflected energy. This situation could be rectified to a large degree by presenting the measurements on a semi-log scale.

The absolute value of the spectral BDR can be calculated from the following expression:

$$\rho_{bd}(\theta',\phi';\theta,\phi) = \rho_o(\theta',\phi')\left[\frac{\rho_s(\theta',\phi')}{\rho_o(\theta',\phi')}\right] \cdot \left[\frac{\rho_{bd}(\theta',\phi';\theta,\phi)\cos\theta}{\rho_{bd}(\theta',\phi';\theta',\phi'+\pi)\cos\theta'}\right]\frac{1}{\cos\theta\,\Delta\omega} \qquad (2.3.1)$$

where the ratio in the first bracket is obtained from Fig. 2b and the second bracket from either Fig. 3, 4, or 5. The specular reflectance of the smooth sample, $\rho_o(\theta',\phi')$ was not measured but an indication of its magnitude can be found in [8] for pure aluminum.

2.3.3 Comparison with a Bidirectional Reflectance Model

Since the measurements reported in Figs. 2b, 3, 4, and 5 exhibit characteristics similar to those predicted by a BDR model based on physical optics, a comparison between the measurements and a physical optics model was made. The BDR model selected is attributed

to Beckmann [9]. Houchens and Hering [10] examined this model in view of certain theoretical criteria and available experimental data and have shown that it has a wider range of application than some other physical optics models. The BDR expression for the Beckmann model can be written in the following general form:

$$\frac{\rho_{bd}(\theta',\phi';\theta,\phi)}{\rho_o(\theta',\phi')} = f_{sp}\left(\theta',\phi';\theta,\phi;\frac{\sigma}{\lambda}\right) F(u) + f_{sc}\left(\theta',\phi';\theta,\phi;\frac{\sigma}{\lambda}, m\right) \qquad (2.3.2)$$

where ρ_o is the specular reflectance of an optically smooth surface and accounts for absorption. f_{sp} is the specular BDR component with F designating that this component has only a non-zero value in the specular direction. f_{sc} is the scattered BDR component, and σ and m are the rms surface roughness height and slope, respectively. Specific expressions for f_{sp}, F, and f_{sc} are available in [10].

In order to compare this model with the measurements, the surface roughness parameters σ and m which according to the model characterize the surface contour must be determined. Since mechanical methods were not available, an optical method based on the measurement of monochromatic specular reflectance was employed [10]. According to Eq. (2.3.2), the monochromatic reflectance in the specular direction may be written as

$$\frac{\rho_s(\theta',\phi')}{\rho_o(\theta',\phi')} = \exp\left[-\left(4\pi\frac{\sigma}{\lambda}\cos\theta'\right)^2\right] + f_{sc}\left(\theta',\phi';\theta',\phi'+\pi;\frac{\sigma}{\lambda}, m\right)\cos\theta'\,\Delta\omega \qquad (2.3.3)$$

For this comparison, ρ_o was taken as the specular reflectance of sample 1. For sufficiently long wavelengths, the scattered component is negligible and Eq. (2.3.3) reduces to

$$\frac{\rho_s(\theta',\phi')}{\rho_o(\theta',\phi')} \simeq \exp\left[-\left(4\pi \frac{\sigma}{\lambda} \cos\theta'\right)^2\right] \tag{2.3.4}$$

where the right-hand side of Eq. (2.3.4) is just the specular component. Thus, a plot of ρ_s/ρ_o versus $1/\lambda^2$ on a semi-log scale is a straight line with slope proportional to σ^2. Measured values of ρ_s/ρ_o for samples 4, 5, and 6 are plotted on a semi-log scale in Fig. 2a as a function of $1/\lambda^2$ for an angle of incidence equal to 10°. Data for long wavelengths was weighted more heavily in locating the straight lines since the assumption of negligible scattered energy is most applicable at these wavelengths. The values of σ obtained from the slopes of the lines are given in TABLE 1. Using these σ values, ρ_s/ρ_o was calculated from Eq. (2.3.4) for each sample and the results are presented as solid curves with the specular reflectance data in Figs. 2b and 2c. The deviation of data and theory at short wavelengths is attributed to the scattered energy effects which become increasingly important at short wavelengths. The broken curves are discussed below.

For short wavelengths, both the specular and scattered energy components in Eq. (2.3.3) are significant. Thus, with σ determined and θ' and $\Delta\omega$ specified, the rms slope can be calculated using the measured values of ρ_s/ρ_o in Eq. (2.3.3). Results of these calculations

are given in TABLE 2 for selected wavelengths. If the model were exact and there were no uncertainties in the measurements, the values for the rms roughness slope m calculated at different wavelengths would be identical. In order to compare the Beckmann model to the data, an average value of m was determined for each sample from those listed in TABLE 2, and these are given in TABLE 1. It is interesting to note that although sample 6 has a rms roughness height more than twice that of sample 5, the rms roughness slope is almost identical to that of sample 5. Verification of the optically determined surface roughness parameters could be obtained from a profilometer trace of the samples; however, this instrument was not available.

Using the σ and average m values given in TABLE 1, ρ_s/ρ_o was calculated from Eq. (2.3.3) for each sample at selected wavelengths. The results are shown in Figs. 2b and 2c as broken curves. For $\sigma/\lambda < 0.1$, the contribution of scattered energy is small, but it increases rapidly until for $\sigma/\lambda > 0.2$, it is nearly the sole contributor to the reflected energy. The limiting value for the scattered energy is determined by rms roughness slope and increases with decreasing m. For $\sigma/\lambda < 0.2$, the agreement between the model and the data is good. For larger values of σ/λ, the model deviates from the data but it has trends similar to the measurements. Some explanation can be given for the discrepancy between the model and data. First, the method used to calculate a unique m value for each sample contributes to the disagreement between the model and the data for large σ/λ. By appropriate selection of m, the model and data could be forced

to coincide at a large σ/λ value. However, for large σ/λ, shadowing effects and multiple reflections which are not accounted for by the model become increasingly important. Thus, it is more appropriate to select m from data for $\sigma/\lambda < 0.2$ where the validity of the model is open to less criticism. Second, the measurement uncertainties are larger at short wavelengths due to low signal to noise ratio. A lead sulfide detector and tungsten source would significantly reduce these uncertainties at wavelengths in the range 0.7-2.8 μm while a photomultiplier detector would accomplish the same for $0.22\ \mu m < \lambda < 0.7\ \mu m$.

Comparison of the spatial distribution of reflected energy calculated from the Beckmann model and the BDR data is shown in Figs. 3, 4, and 5. The solid curves were calculated from Eq. (2.3.2) using the σ and m values given in TABLE 1. The broken curves represent the scattered component. Considering its limitations, the model exhibits characteristics similar to the data for illumination at near normal incidence.

Of particular interest is that although samples 4 and 6 have identical values of σ/λ at wavelengths of 2.4 μm and 6.4 μm, respectively, the distributions shown in Figs. 3b and 5c indicate that sample 4 is smoother than sample 6. Furthermore, sample 6 has an optical roughness of approximately twice that of sample 5 for a wavelength of 1.4 μm. According to [11], sample 6 would be expected to scatter a larger amount of the incident energy than sample 5. However, the distributions for the two samples shown in Figs. 4a and

5a at a wavelength of 1.4 μm are nearly identical. Hence, it appears that optical roughness alone is insufficient to characterize the BDR of a rough surface. This is contrary to the findings of some investigators [11]. According to the Beckmann model, the rms slope must also be specified in order to obtain an indication of the BDR. Further experimental verification of the importance of the rms roughness slope is needed.

2.3.4 Conclusions

The BDR measurements reported have demonstrated that the reflectometer has the desired capabilities. Signal levels obtained for the wavelength range 2-14 μm and for the slit width-solid angle combinations employed were sufficiently far removed from system noise to enable meaningful measurements to be made. For wavelengths greater than 14 μm, it is necessary to use larger solid angles and/or operate the monochromator in the single pass mode with an external chopper to avoid noise problems. For wavelengths less than 2 μm, it is necessary to employ other detectors and sources.

Available surface preparation and specification techniques were severely limited. Additional grit sizes and metal samples would be useful in preparing surfaces of different roughnesses. It was concluded that a profilometer measurement of surface topography would provide the most useful means for evaluating surface roughness parameters. However, the feasibility of using a scanning electron microscope for surface contour measurements is being investigated. These

parameters could also be used to verify those calculated from optical measurements and a BDR model.

The methods of accounting for absorption of incident energy can be investigated by using a roughened sample with coatings of different materials. A measurement which was not available for this study and is required to investigate methods of accounting for absorption is the directional hemispherical reflectance. This measurement is particularly important for substantiating a BDR model based on physical optics.

3. FUTURE RESEARCH

Future efforts in theoretical studies will concentrate first on intensive analysis of the numerical results obtained from the real surface radiant transfer study utilizing the detailed bidirectional reflectance models. All details and quantitative results of this analysis as well as the important conclusions drawn therefrom will be submitted shortly in a report devoted entirely to this study.

Analytical studies of surface roughness effects on radiant heat transfer and equilibrium temperature of grooved surfaces will continue. Computations for both radiant transfer and radiant exchange for the parallel plate geometry are underway and upon completion will delineate the influence of surface roughness on radiative transfer for systems of widely different interaction characteristics. Subsidiary analyses and computations are also being initiated to investigate the accuracy of simple surface reflection models in predicting rough surface radiant transfer. This effort is expected to be completed within the next six-month contract period. The extension of the adjoint plate system code to include solar flux, thereby permitting evaluation of surface roughness effects on equilibrium temperature, is underway and will be continued.

The bidirectional reflectance measurement facility is presently being upgraded to automatically scan over all directions of reflected energy in the plane of incidence. Turntables, stepping motors, and a controller have been purchased and delivery is expected shortly.

In addition, a digital data acquisition and recording system has been selected. Finally, problems with erratic rotation of the chopper motor in the monochromator are being alleviated by replacing the original motor with a synchronous motor. Bidirectional reflectance measurements in the plane of incidence for surfaces with well-defined roughness characteristics, as well as for other selected samples will commence upon completion of the system improvements.

4. REFERENCES

1. R. G. Hering, A. F. Houchens, T. F. Smith, W. D. Fischer, and G. Hill, "Radiant Heat Exchange in a Space Environment," Scientific Technical Report No. 2, Contract No. 951661, Jet Propulsion Laboratory, California Institute of Technology (1967).

2. R. G. Hering, A. F. Houchens, T. F. Smith, and W. D. Fischer, "Radiant Heat Exchange in a Space Environment," Scientific Technical Report No. 3, Contract No. 951661, Jet Propulsion Laboratory, California Institute of Technology (1968).

3. R. G. Hering, A. F. Houchens, T. F. Smith, and W. D. Fischer, "Radiant Heat Exchange in a Space Environment," Scientific Technical Report No. 4, Contract No. 951661, Jet Propulsion Laboratory, California Institute of Technology (1968).

4. R. C. Birkebak and E. R. G. Eckert, "Effects of Roughness of Metal Surfaces on Angular Distribution of Monochromatic Reflected Radiation," J. Heat Transfer, Trans. ASME 87C, 85 (1965).

5. K. E. Torrance and E. M. Sparrow, "Biangular Reflectance of an Electric Nonconductor as a Function of Wavelength and Surface Roughness," J. Heat Transfer, Trans. ASME 87C, 283 (1965).

6. H. E. Bennett and J. O. Porteus, "Relation Between Surface Roughness and Specular Reflectance at Normal Incidence," J. Opt. Soc. Am. 51, 123 (1961).

7. K. E. Torrance, "Off-Specular Peaks and Angular Distribution of Reflected Thermal Radiation," Ph.D. Dissertation, Mechanical Engineering Department, University of Minnesota, Minneapolis, Minnesota (1966).

8. G. Hass, "Optical Properties of Metals," in American Institute of Physics Handbook, Second Edition, McGraw-Hill Book Co., Inc., New York, pp. 6-107 (1963).

9. P. Beckmann and A. Spizzichino, The Scattering of Electromagnetic Waves from Rough Surfaces, The Macmillan Co., New York (1963).

10. A. F. Houchens and R. G. Hering, "Bidirectional Reflectance of Rough Metal Surfaces," AIAA Series Progress in Astronautics and Aeronautics: Thermophysics of Spacecraft and Planetary Bodies 20, 65 (1967).

11. K. E. Torrance and E. M. Sparrow, "Off-Specular Peaks in the Directional Distribution of Reflected Thermal Radiation," J. Heat Transfer, Trans. ASME 88C, 223 (1966).

5. FIGURES AND TABLES

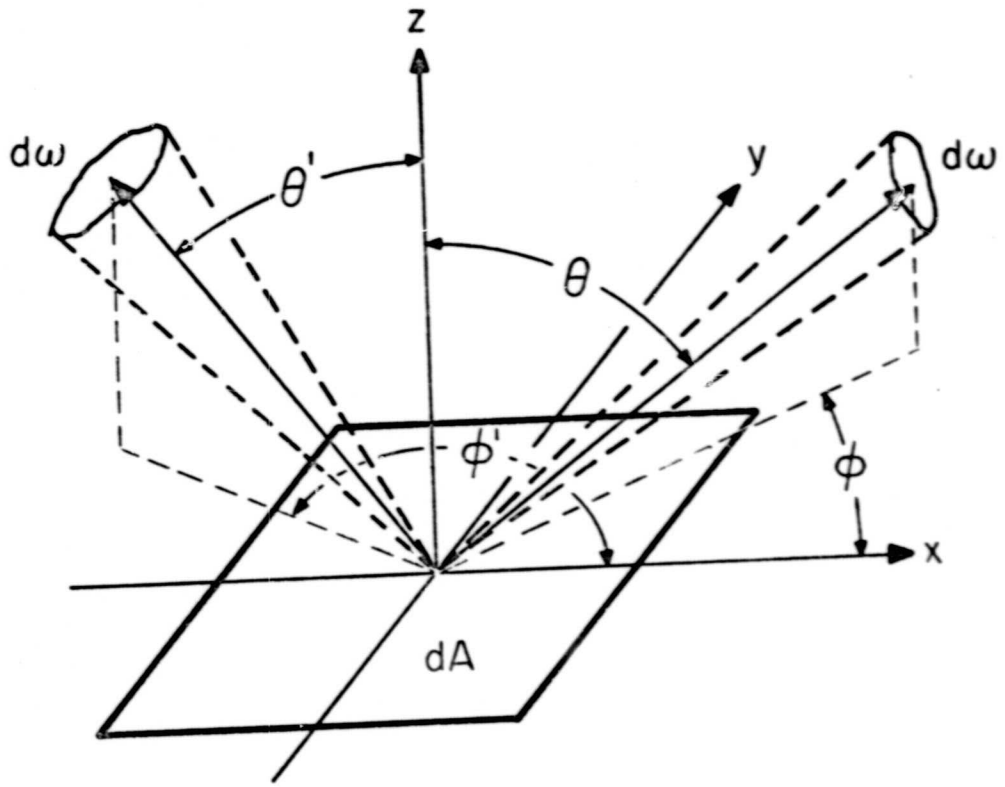

Figure 1. Angles of Incidence and Reflection

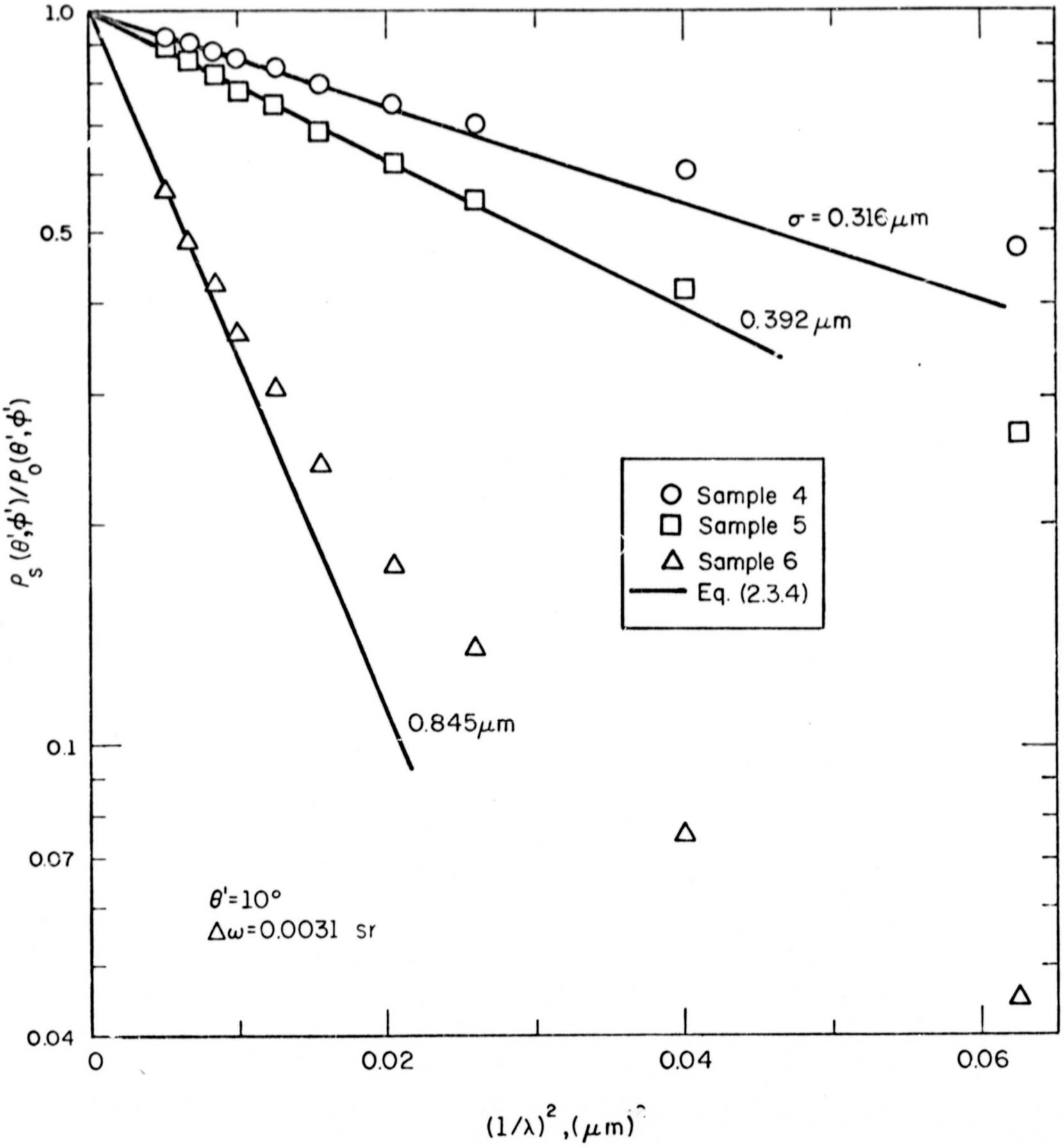

Figure 2a

Evaluation of rms Surface Roughness Height σ Using Specular Component of Beckmann Model

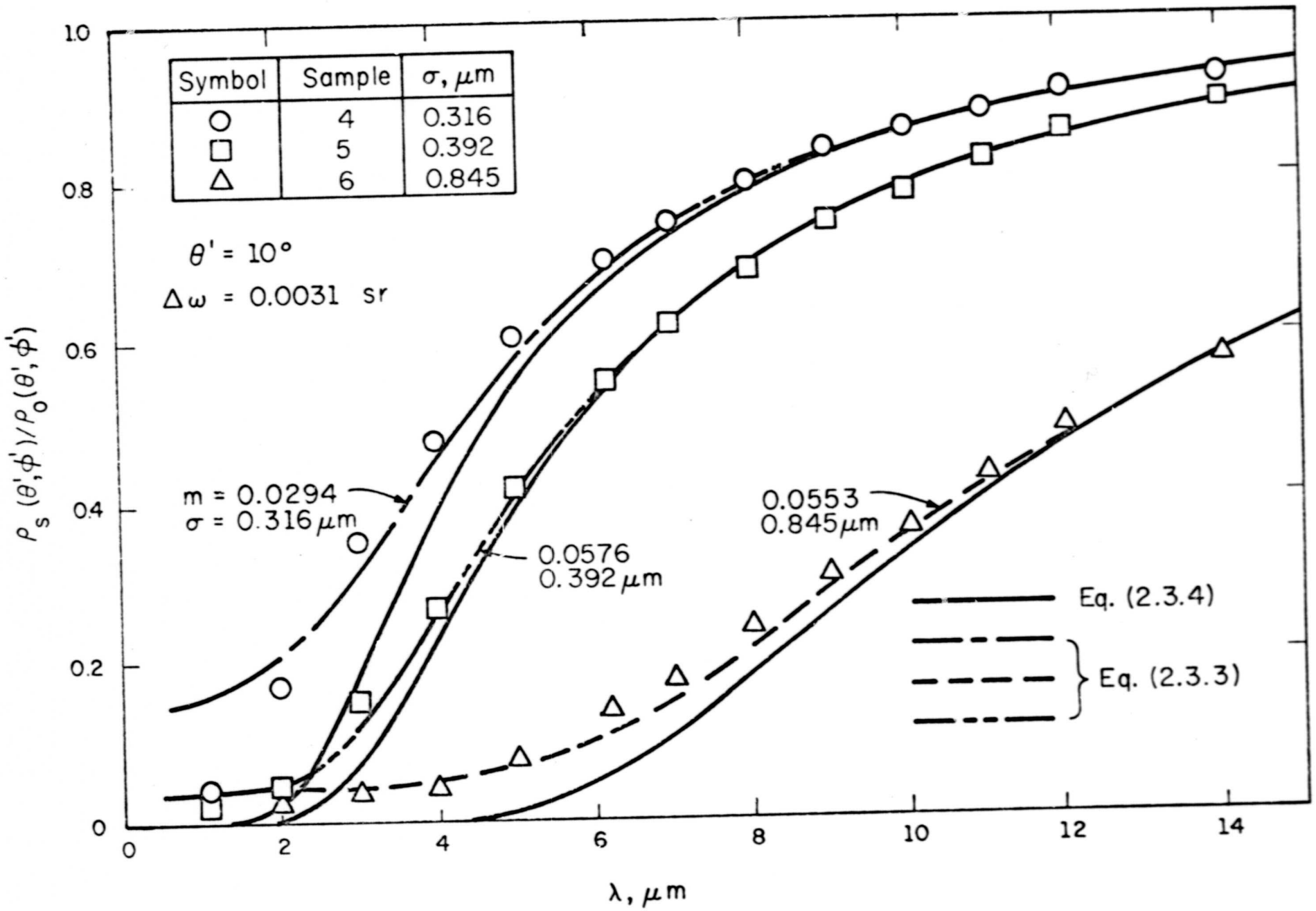

Figure 2b
Comparison of Specular Reflectance Data with Beckmann Model

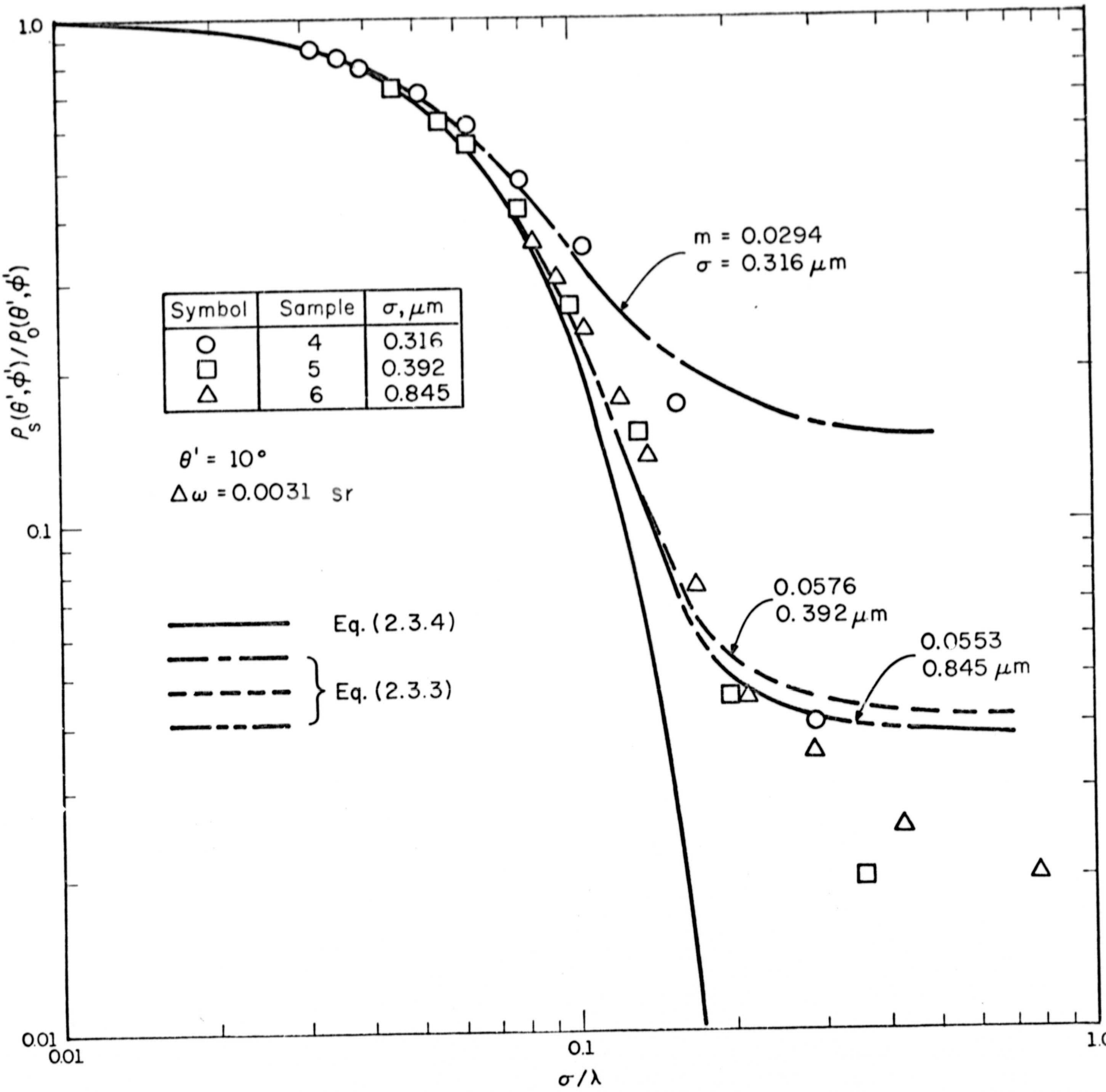

Figure 2c

Comparison of Specular Reflectance Data with Beckmann Model

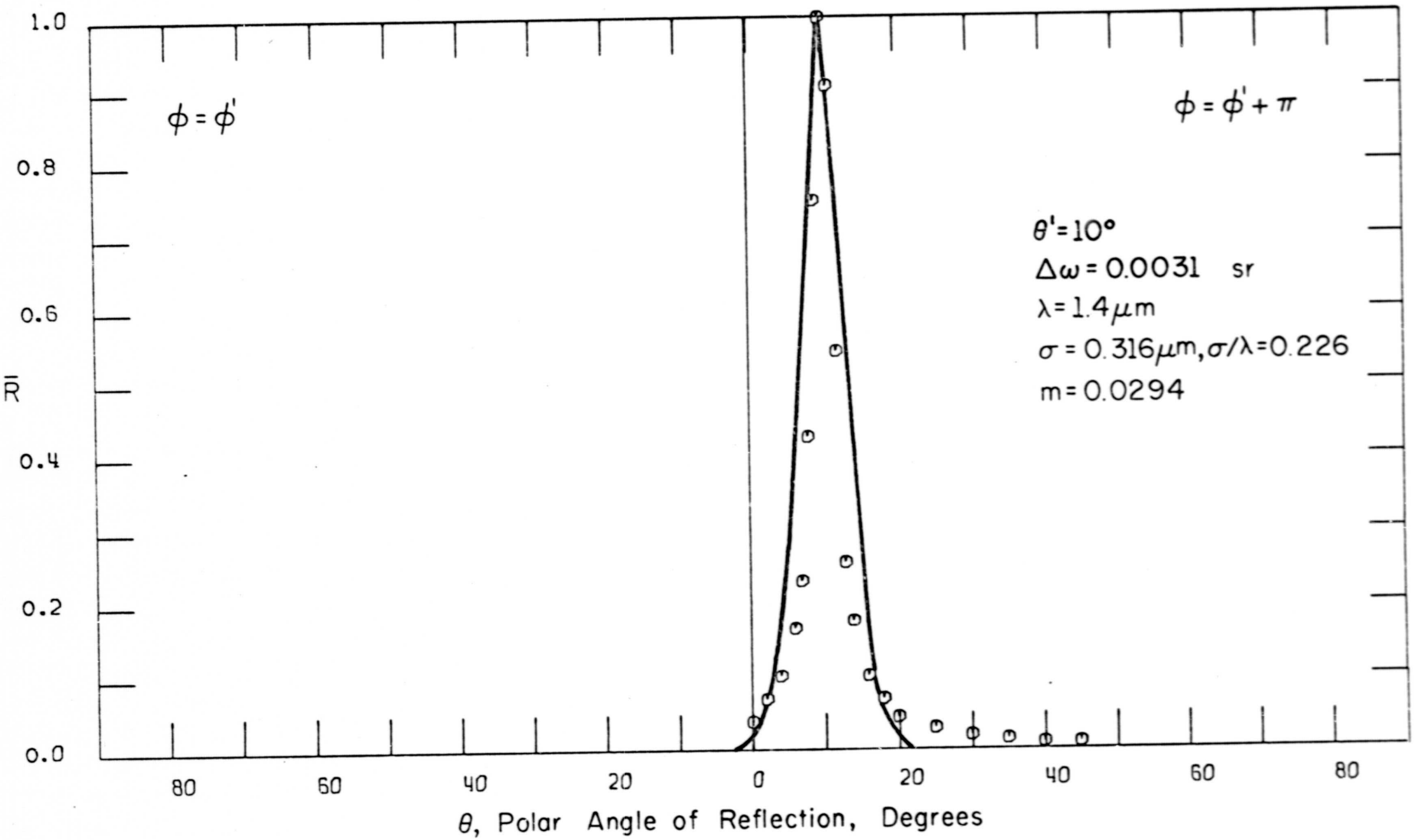

Figure 3a

Comparison of Bidirectional Reflectance Data with Beckmann Model at λ = 1.4μm--Sample 4

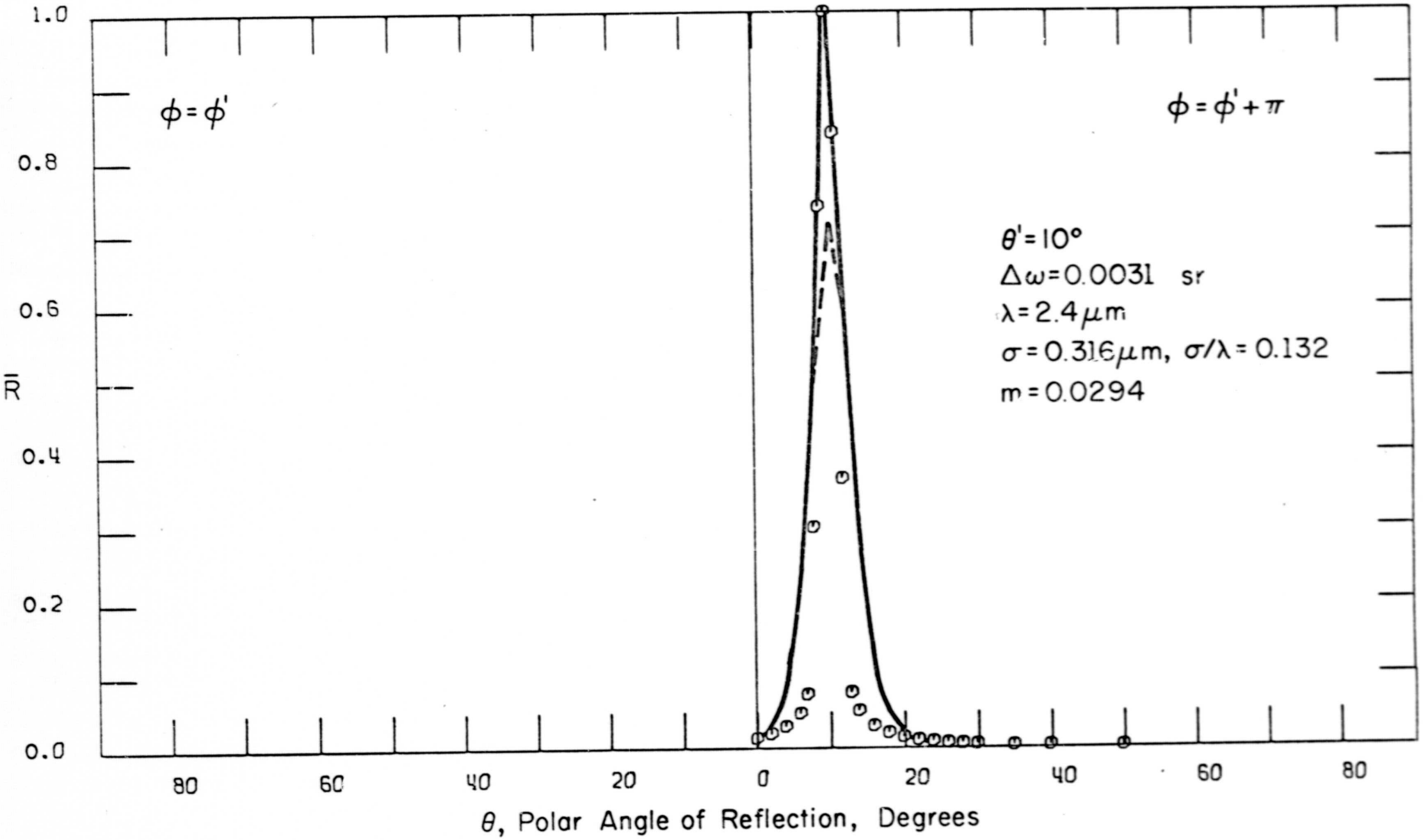

Figure 3b

Comparison of Bidirectional Reflectance Data with Beckmann Model at λ = 2.4μm--Sample 4

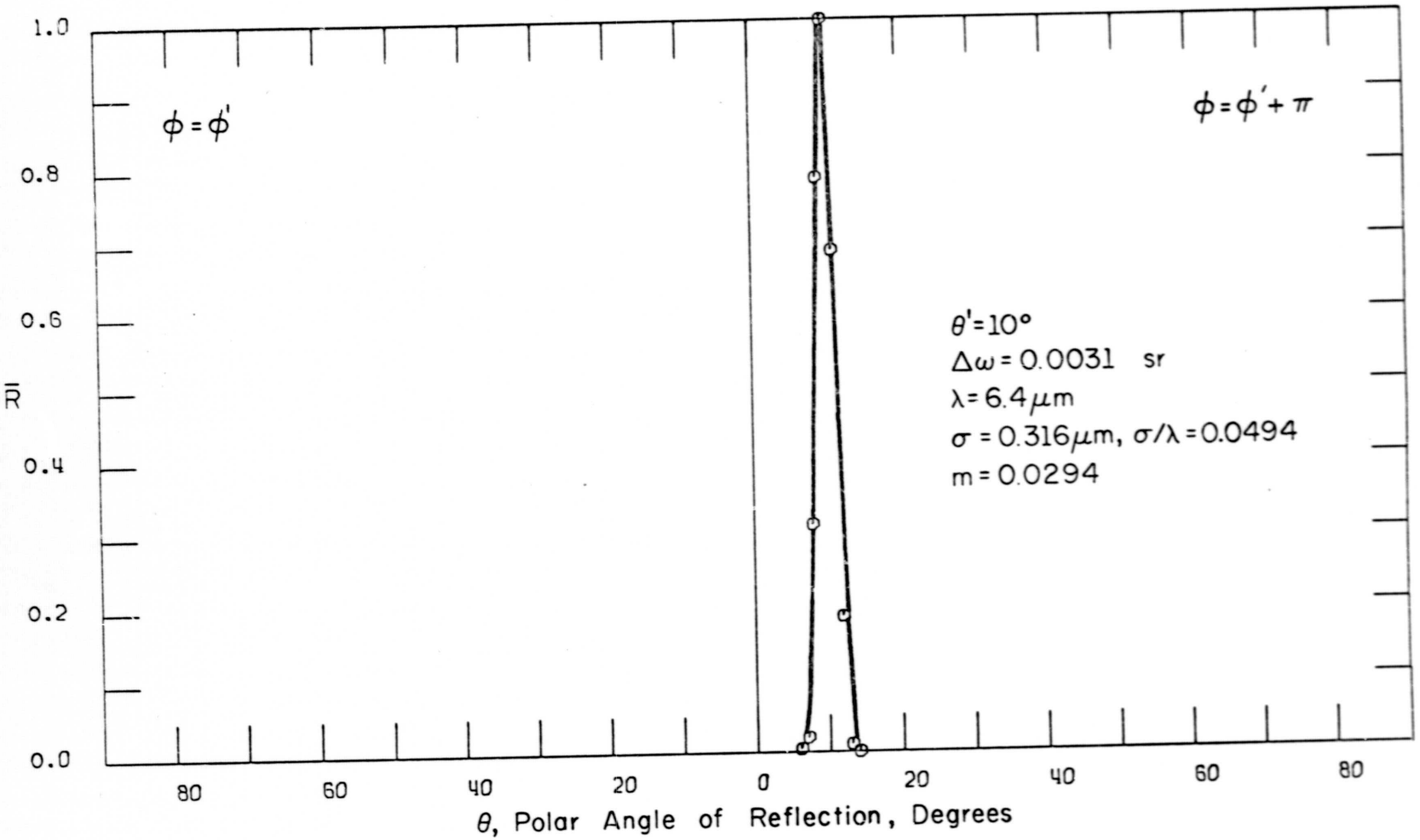

Figure 3c

Comparison of Bidirectional Reflectance Data with Beckmann Model at λ = 6.4μm--Sample 4

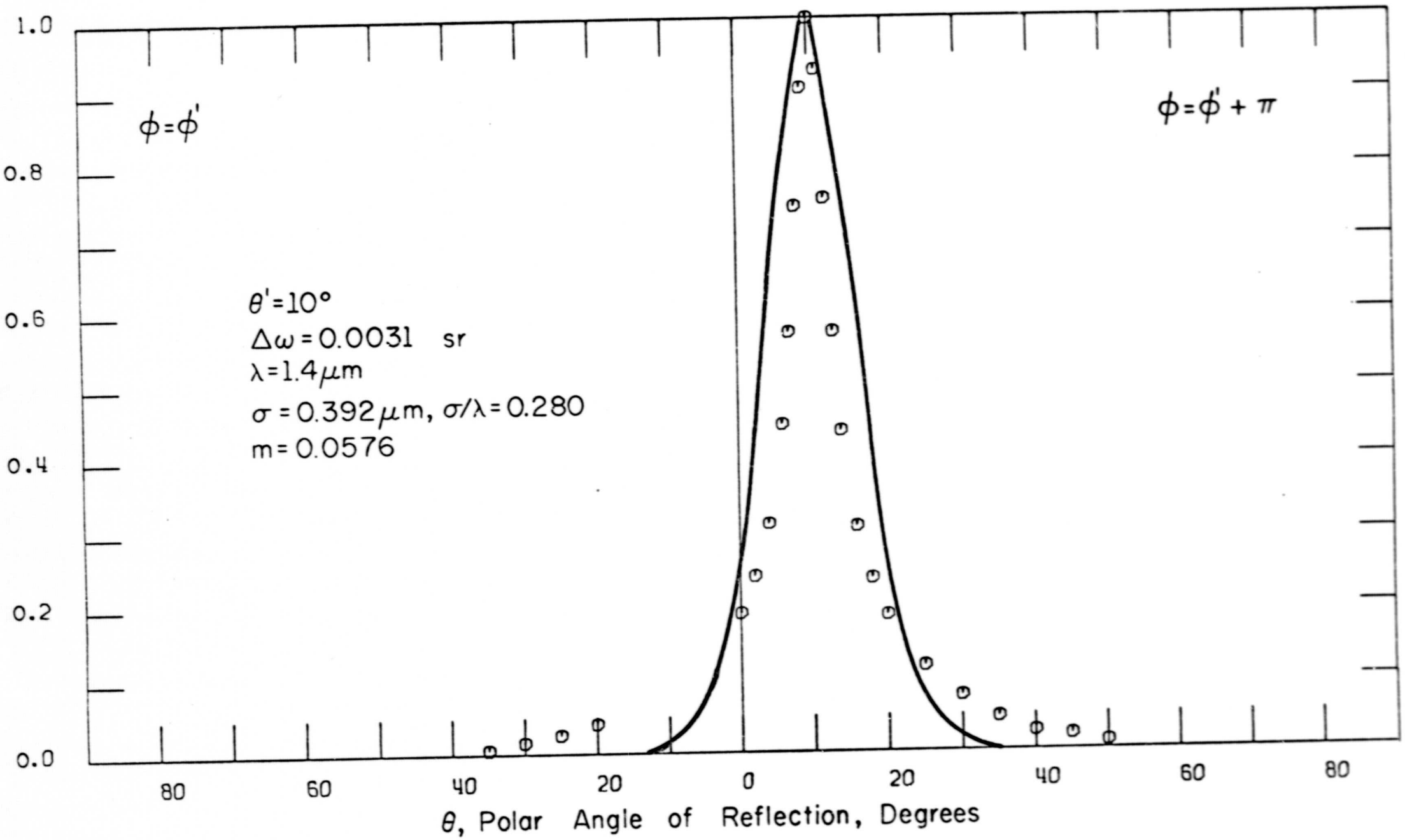

Figure 4a

Comparison of Bidirectional Reflectance Data with Beckmann Model at λ = 1.4μm--Sample 5

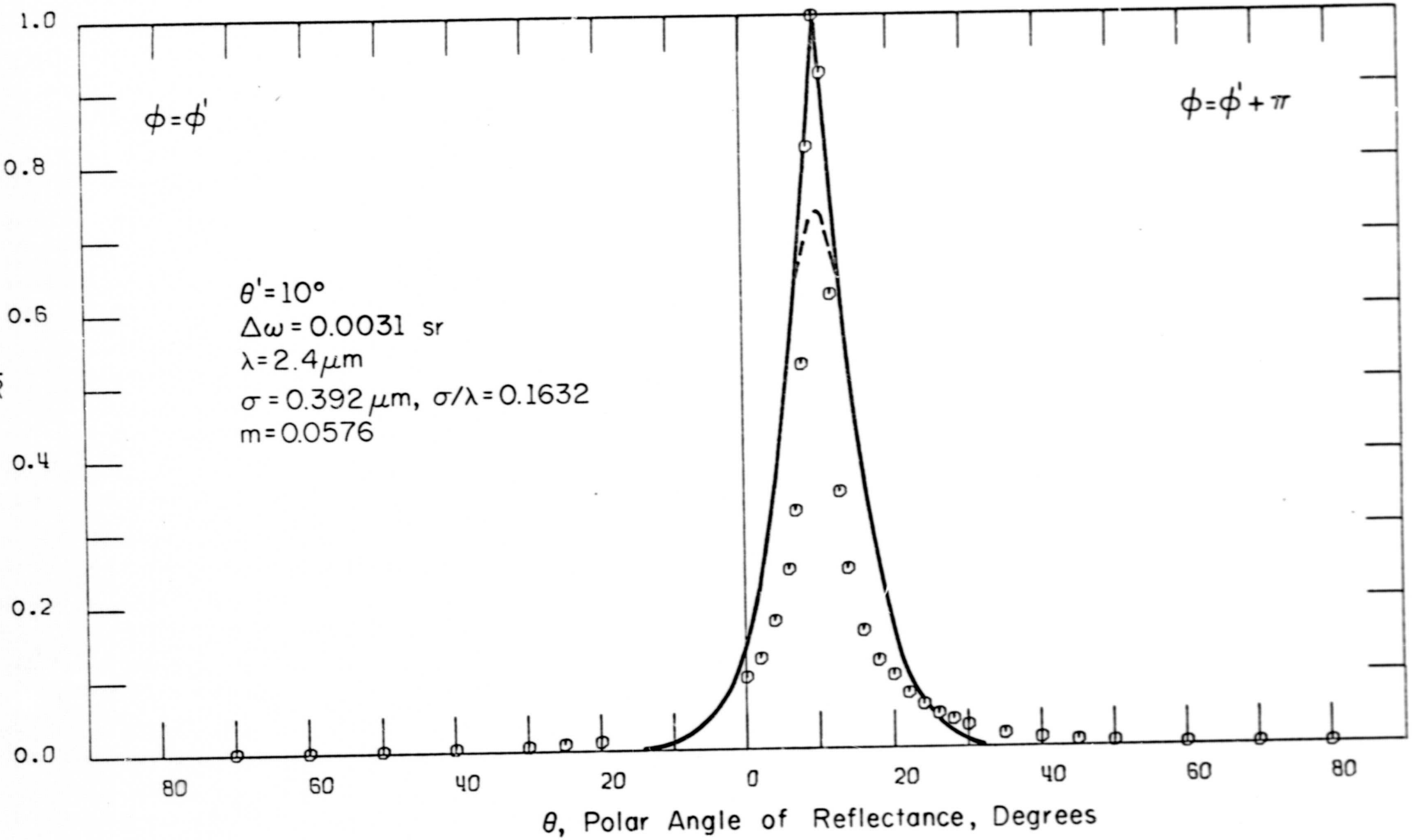

Figure 4b

Comparison of Bidirectional Reflectance Data with Beckmann Model at λ = 2.4μm--Sample 5

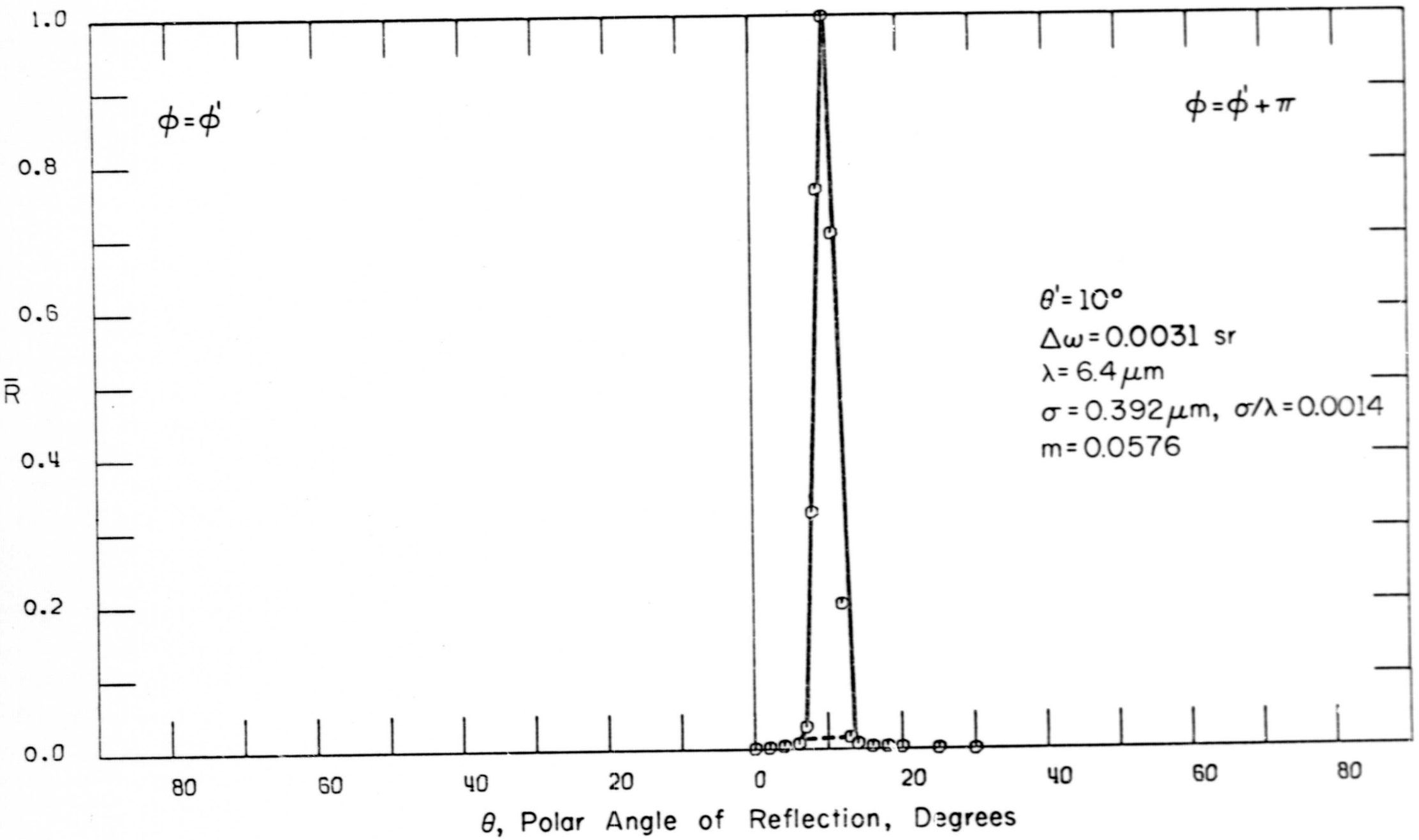

Figure 4c

Comparison of Bidirectional Reflectance Data with Beckmann Model at λ = 6.4μm--Sample 5

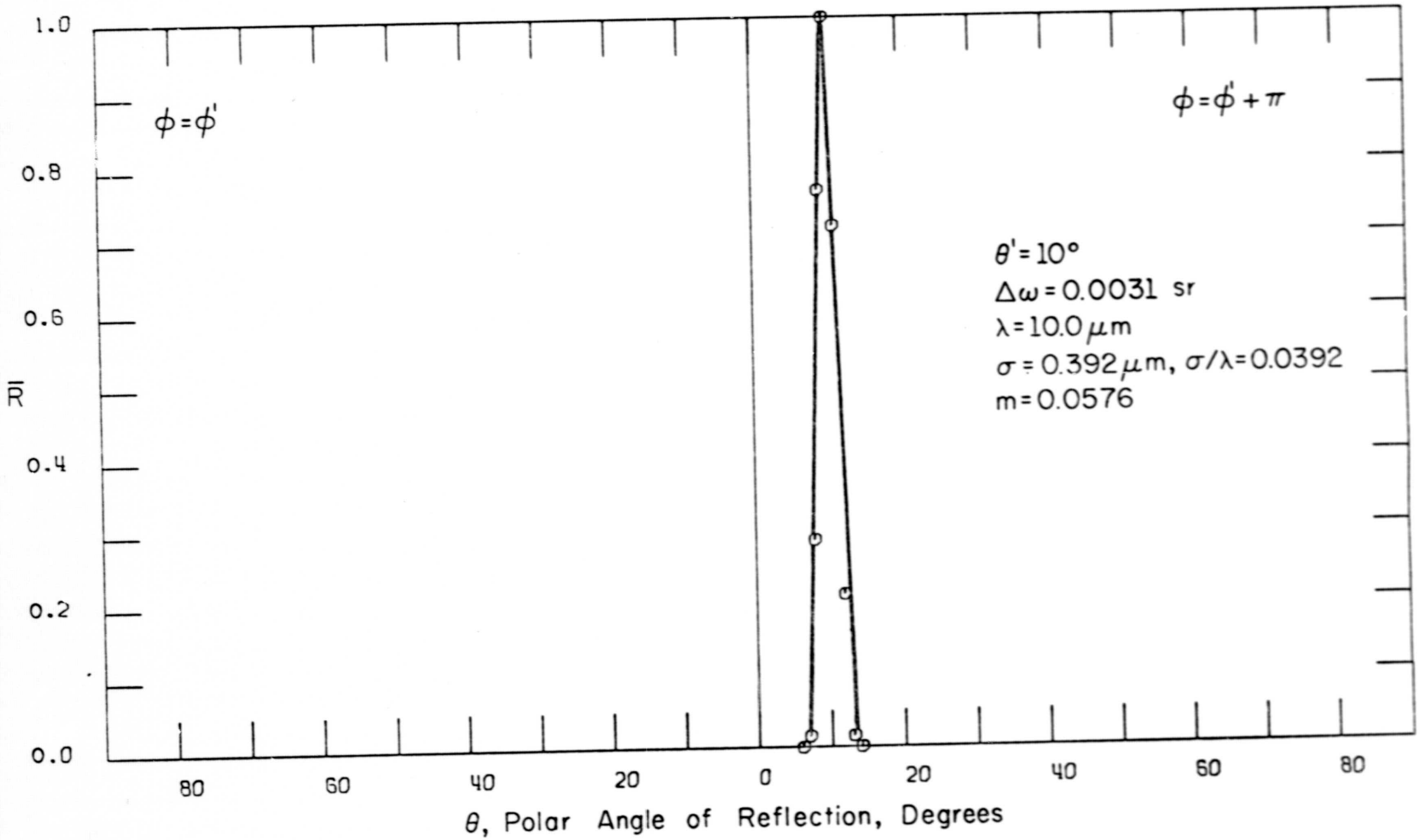

Figure 4d

Comparison of Bidirectional Reflectance Data with Beckmann Model at λ = 10μm--Sample 5

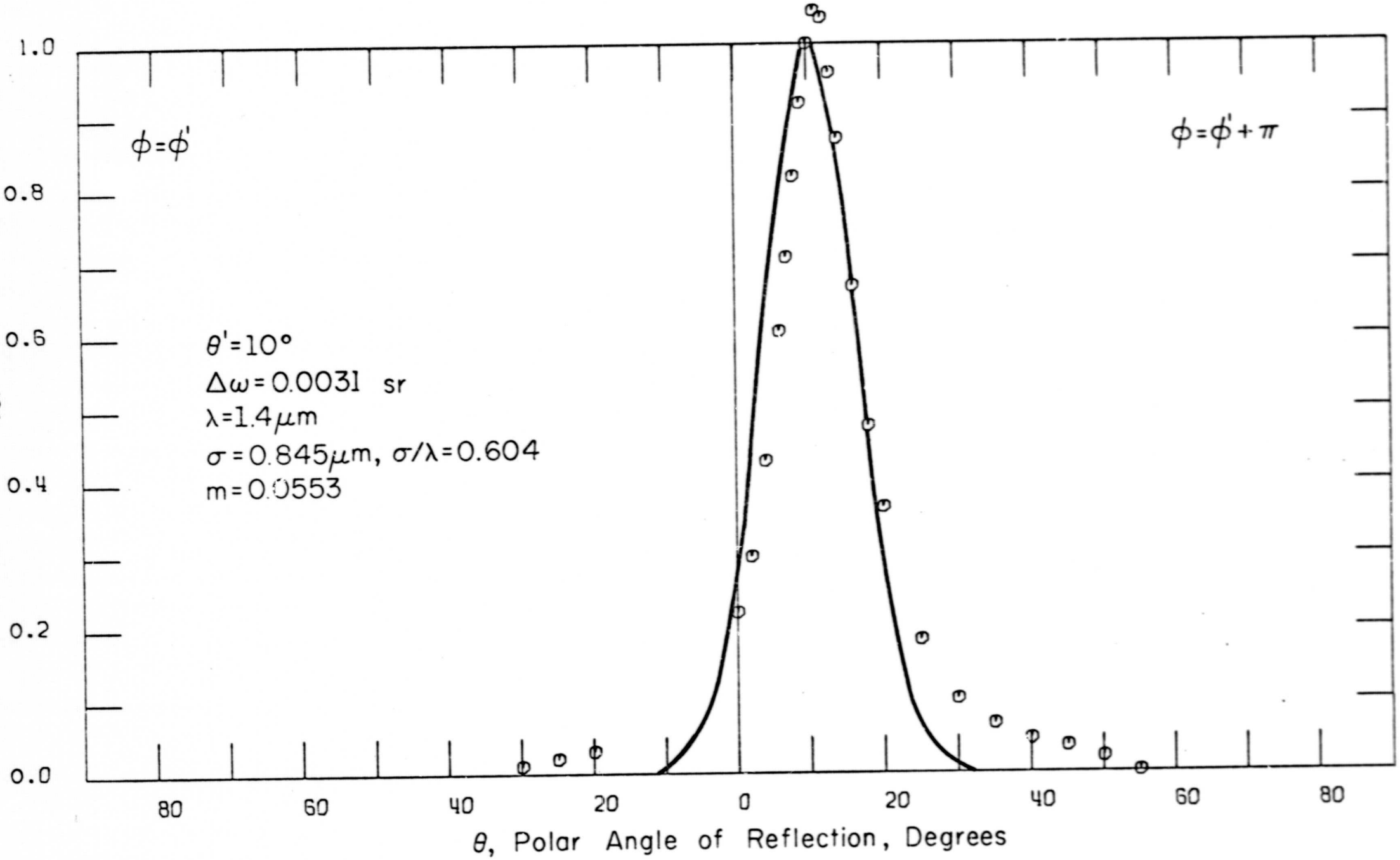

Figure 5a

Comparison of Bidirectional Reflectance Data with Beckmann Model at λ = 1.4μm--Sample 6

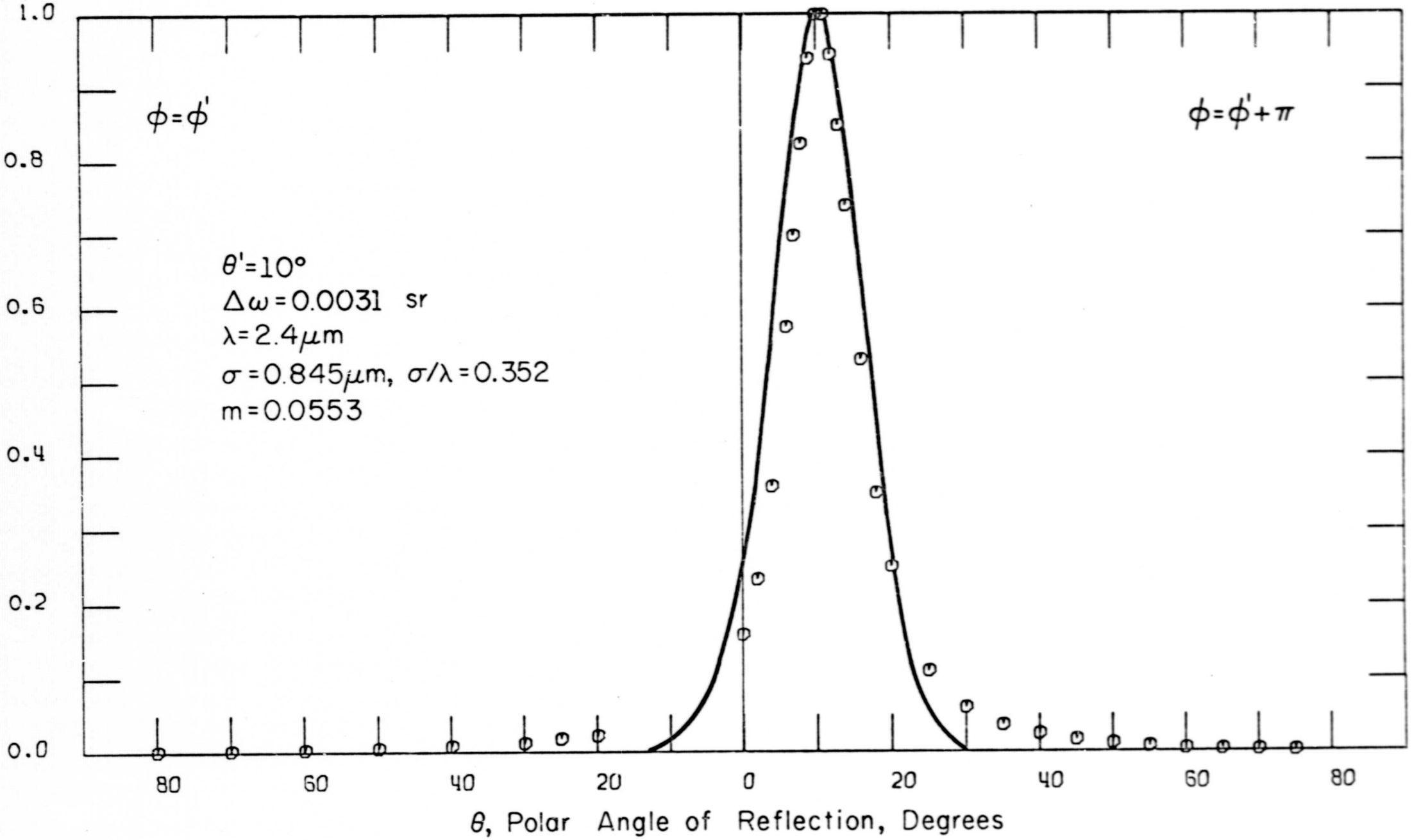

Figure 5b

Comparison of Bidirectional Reflectance Data with Beckmann Model at λ = 2.4μm--Sample 6

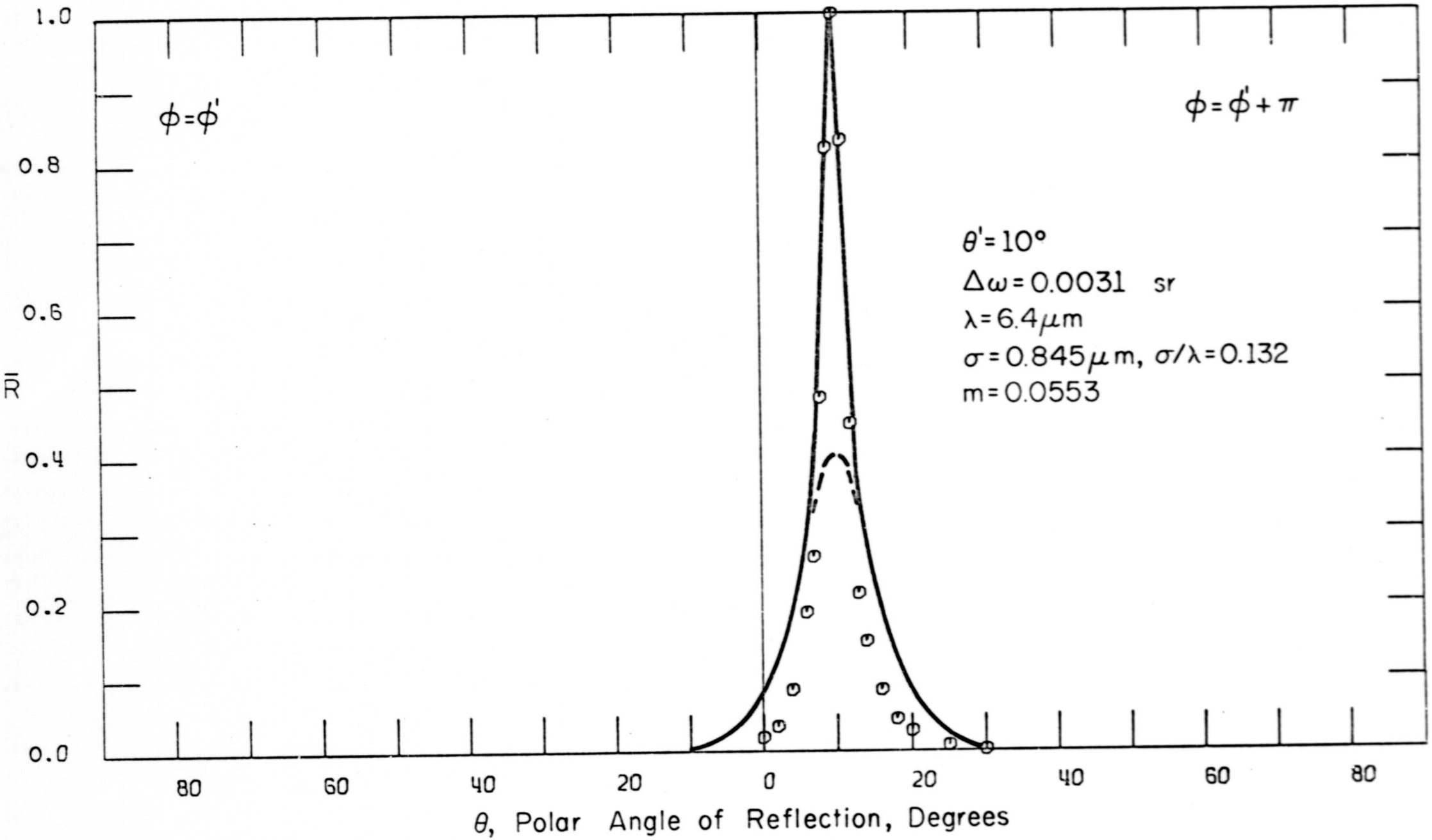

Figure 5c

Comparison of Bidirectional Reflectance Data with Beckmann Model at λ = 6.4μm--Sample 6

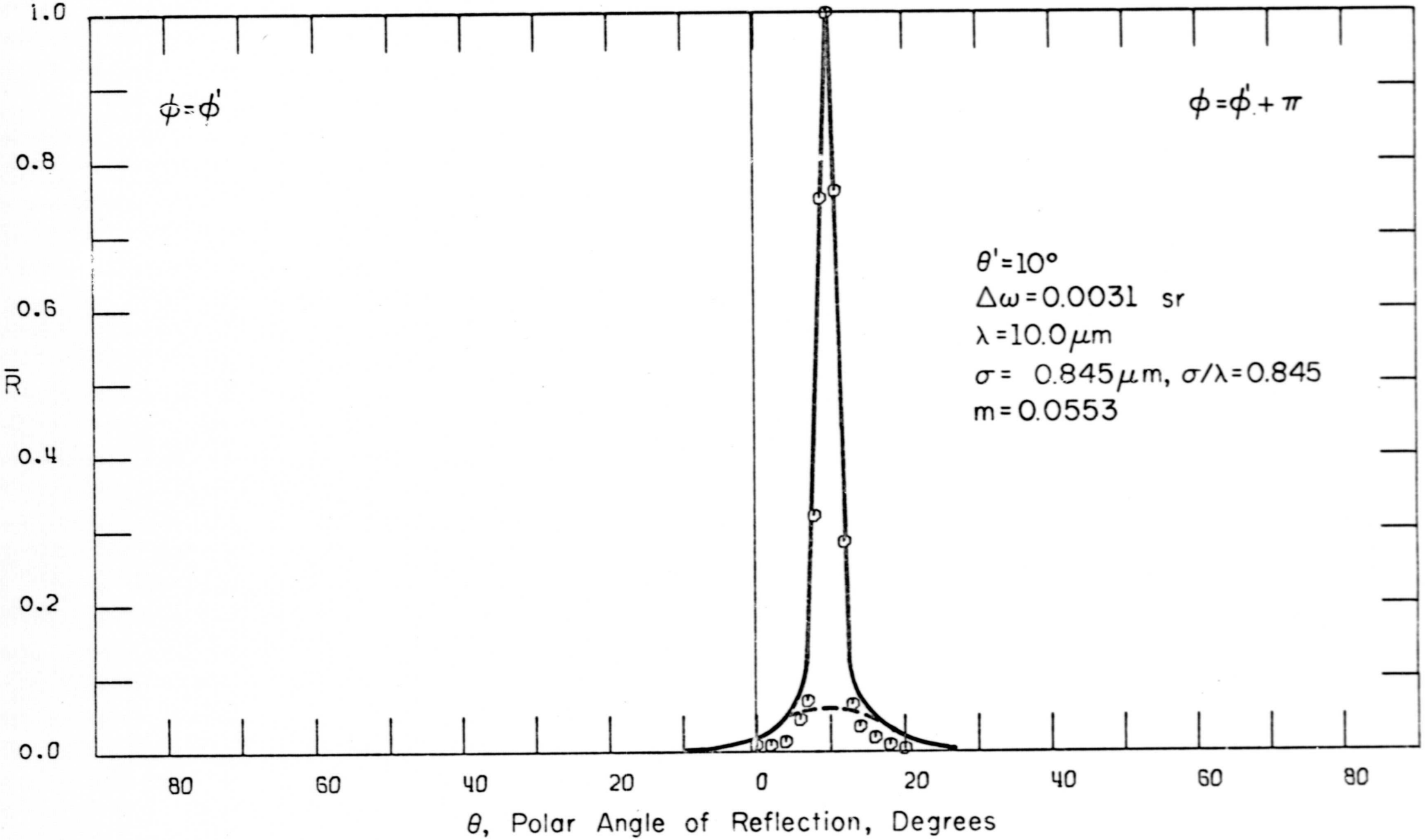

Figure 5d

Comparison of Bidirectional Reflectance Data with Beckmann Model at λ = 10.0μm--Sample 6

TABLE 1

SAMPLE DESIGNATION, MEAN GRINDING GRIT SIZES AND rms ROUGHNESS PARAMETERS

Sample Number	Mean Grit Sizes (μm)	rms Surface Roughness Height, σ (μm)	rms Surface Roughness Slope, m
1	0.05	--	--
2	0.3	--	--
3	15.0	--	--
4	19.0	0.316	0.0294
5	30.0	0.392	0.0576
6	54.0	0.845	0.0553

TABLE 2

VALUES FOR rms ROUGHNESS SLOPE

Sample 4, σ = 0.316 μm			Sample 5, σ = 0.392 μm			Sample 6, σ = 0.845 μm		
λ, μm	σ/λ	m	λ, μm	σ/λ	m	λ, μm	σ/λ	m
1.1	0.2870	0.0583	1.1	0.3560	0.0810	1.1	0.7680	0.0792
2.0	0.1580	0.0329	2.0	0.1960	0.0606	2.0	0.4230	0.0718
3.0	0.1050	0.0254	3.0	0.1310	0.0435	3.0	0.2820	0.0625
4.0	0.0790	0.0251	4.0	0.0980	0.0517	4.0	0.2110	0.0585
5.0	0.0632	0.0218	5.0	0.0740	0.0472	5.0	0.1690	0.0507
6.2	0.0510	0.0228	6.2	0.0632	0.0614	6.2	0.1360	0.0442
7.0	0.0451	0.0270				7.0	0.1210	0.0414
8.0	0.0295	0.0280				8.0	0.1060	0.0430
9.0	0.0351	0.0233				9.0	0.0939	0.0434